Journal of Biomechanics 90 (2019) 71–77

Contents lists available at ScienceDirect

Journal of Biomechanics

journal homepage: www.elsevier.com/locate/jbiomech
www.JBiomech.com

Estimates of Achilles tendon moment arm differ when axis of ankle rotation is derived from ankle motion

Francesca E. Wade [a], Gregory S. Lewis [b,c], Stephen J. Piazza [a,b,c,*]

[a] Biomechanics Laboratory, Department of Kinesiology, The Pennsylvania State University, University Park, PA 16802, USA
[b] Department of Mechanical and Nuclear Eng., The Pennsylvania State University, University Park, PA 16802, USA
[c] Department of Orthopaedics and Rehabilitation, The Pennsylvania State University, Hershey, PA 17033, USA

ARTICLE INFO

Article history:
Accepted 22 April 2019

Keywords:
Moment arm
Axis of rotation
Ankle
Achilles tendon
Ultrasound

ABSTRACT

The plantarflexor moment arm of the Achilles tendon determines the mechanical advantage of the triceps surae and also indirectly affects muscle force generation by setting the amount of muscle-tendon shortening per unit of ankle joint rotation. The Achilles tendon moment arm may be determined geometrically from an axis (or center) of joint rotation and the line of action of the tendon force, but such moment arms may be sensitive to the location of the joint axis. Using motion analysis to track an ultrasound probe overlying the Achilles tendon along with markers on the shank and foot, we measured Achilles tendon moment arm during loaded and unloaded dynamic plantarflexion motions in 15 healthy subjects. Three representations of the axis or center of rotation of the ankle were considered: (1) a functional axis, defined by motions of the foot and shank; (2) a transmalleolar axis; and (3) a transmalleolar midpoint. Moment arms about the functional axis were larger than those found using the transmalleolar axis and transmalleolar midpoint (all $p < 0.001$). Moment arms computed with the functional axis increased with plantarflexion angle (all $p < 0.001$), and increased with loading in the most plantarflexed position ($p < 0.001$) but these patterns were not observed when either using a transmalleolar axis or transmalleolar midpoint. Functional axis moment arms were similar to those estimated previously using magnetic resonance imaging, suggesting that using a functional axis for ultrasound-based geometric estimates of Achilles tendon moment arm is an improvement over landmark-based methods.

1. Introduction

The plantarflexor moment arm of the Achilles tendon affects plantarflexor function through its combined influence on both leverage and muscle fiber length and shortening velocity, both of which affect muscle force generation. The plantarflexion moment arm of the Achilles tendon (ATma) determines the mechanical advantage of the triceps surae relative to the ground reaction force during the latter part of stance phase in activities requiring transmission of calf muscle forces (Carrier et al., 1994). In addition, ATma determines the extent of muscle fiber shortening for a given ankle joint rotation (Lieber and Ward, 2011), and thus affects plantarflexor muscle operating points on the muscle force-length and force-velocity curves. Because ATma determines plantarflexor muscle moment and force generation, it is a critical determinant of the mechanics of push-off during gait (Rasske et al., 2017; Takahashi et al., 2016).

ATma may be found experimentally as a geometric distance on a two-dimensional (2D) magnetic resonance (MR) image of the ankle joint (Baxter and Piazza, 2014; Maganaris et al., 1998; Rugg et al., 1990). In the 2D geometric method, the center of rotation (CoR) between the tibia and talus is found from images of the ankle made with the ankle in different positions, and the ATma is taken to be the shortest distance from the CoR to the midline of the Achilles tendon. ATma have also been found from three-dimensional (3D) MR images of the ankle complex, either using dynamic cine-MR (Sheehan, 2012) or static images (Clarke et al., 2015).

Ultrasound imaging of the Achilles tendon has also been employed to make estimates of ATma. Muscle moment arm may be found from measurements of tendon excursion and joint angle (Storace and Wolf, 1979), and many investigators have used this tendon excursion method to determine ATma (e.g. Fath et al., 2010; Ito et al., 2000; Spoor and van Leeuwen, 1992). The tendon excursion method does not require the location of a CoR, but does

* Corresponding author at: Biomechanics Laboratory, 29 Recreation Building, The Pennsylvania State University, University Park, PA 16802, USA.
E-mail address: piazza@psu.edu (S.J. Piazza).

https://doi.org/10.1016/j.jbiomech.2019.04.032
0021-9290/

assume that all tendon excursion is attributable to joint rotation rather than tendon stretch and relaxation that are difficult to quantify *in vivo* (Olszewski et al., 2015). For this reason, the tendon excursion method as currently implemented may not be appropriate for quantifying ATma during functional activities. Manal et al. (2010) described a hybrid method combining dynamic ultrasound imaging of the Achilles tendon with 3D tracking of the markers placed on the foot, the tibia, and the ultrasound probe. The Achilles tendon was located from ultrasound images while the motion data were used to identify and track the CoR, which was taken to be the midpoint between the medial and lateral malleoli. The ATma was then estimated throughout the motion by finding the shortest 3D distance between the CoR and the tendon midline. The combination of ultrasound imaging and motion tracking employed in this way allows for dynamic assessment of ATma during weight-bearing tasks such as walking (Rasske et al., 2017).

Results from studies using the hybrid method have produced ATma estimates that differ from those in MR-based studies, potentially due to errors in the location of the CoR. In both 2D and 3D MR studies, ATma has been found to be 8–15 mm larger during muscle contraction (Hashizume et al., 2014; Maganaris et al., 2000). Differences in ATma between conditions of maximum voluntary contraction and rest (Manal et al., 2013) and between stance and swing phase during walking (Rasske et al., 2017), however, have been found to be substantially smaller when hybrid methods have been used. MR-based estimates of ATma have also consistently shown ATma to increase with plantarflexion angle (Hashizume et al., 2012; Maganaris, 2004; Sheehan, 2012), a trend that has not been evident when hybrid methods that assume a transmalleolar midpoint CoR have been used (Franz et al., 2018; Manal et al., 2013; Rasske et al., 2017).

Previous efforts to assess ATma geometrically using ultrasound have specified the CoR as the transmalleolar midpoint (Manal et al., 2013; Rasske et al., 2017). While studies of relative bone motions have found that the CoR is well approximated by a transmalleolar midpoint (Siston et al., 2005), others have revealed differences between the landmark-based transmalleolar axis and the axis of tibiotalar rotation (Lundberg et al., 1989; Lundberg and Svensson, 1993; Sammarco, 1977). A rotation axis derived from marker-based tracking of the relative motion of the foot and shank might better represent the true axis of tibiotalar rotation and thus permit better estimates of ATma.

The purpose of this study was to investigate differences in ATma determined using the ultrasound-motion analysis approach subject to three different methods for approximating the axis or center of ankle rotation. Specifically, we sought to compare ATma results from experiments in which a 'functional axis' is computed from measured ankle motion to results from the same trials in which the axis or center of rotation is determined using markers placed on the malleoli. The three representations of the ankle axis or center of rotation considered were: (1) functional axis (FA) identified using finite helical axis decomposition of the relative motions of the foot and shank; (2) transmalleolar axis of rotation (TA) through markers placed over the medial and lateral malleoli; and (3) the midpoint between the malleolar markers (TM). We hypothesized that: (i) ATma from FA will be larger than those estimated using TA or TM; (ii) a larger change in ATma will be seen with plantarflexion angle using FA than with TM or TA; and (iii) ATma computed with FA will increase with loading to a greater extent than will ATma computed with TM or TA.

2. Methods

Fifteen healthy young adults (8 F, 7 M; age: 26 ± 2 y; height: 1.70 ± 0.07 m; mass: 71 ± 12 kg) were recruited to participate in the study. The protocol was approved by the Institutional Review Board of The Pennsylvania State University, with informed consent obtained prior to data collection for each participant.

Calibration: In order to locate the tendon within the laboratory frame of reference, a static transformation between a reference frame defined by markers attached to the ultrasound probe frame and a frame aligned with the planar ultrasound image was found using a calibration procedure prior to data collection for each subject. Briefly, three cylindrical rod phantoms were imaged underwater using a 60 mm linear ultrasound probe (Telemed HL9.0/60/128Z-2; Lithuania). Retroreflective markers rigidly attached to either end of each rod and four markers attached to the ultrasound probe determined the locations of the rods and the probe in the laboratory reference frame. The centers of the intersections of each rod with the imaging plane were identified and used to create a homogeneous transformation between the probe and image frames. Further details of this calibration procedure are provided in the supplemental materials.

Motion trials: Following probe calibration, 12 mm-diameter retroreflective markers were attached with double-sided tape on the right lower limb over both malleoli and both femoral epicondyles. Two four-marker clusters on molded plastic plates were affixed to the anterior shank and the dorsum of the foot using double-sided tape and elastic wrap (3M Coban; St. Paul, MN). The Achilles tendon was imaged with the middle of the ultrasound probe placed vertically at the level of the malleoli and with the probe oriented to maximize the appearance of the tendon in the image (Fig. 1). The probe was secured in place with a neoprene brace and foam support to minimize the motion of the probe relative to the leg (Fig. 2). Participants performed standing toe raises in time to a metronome at 0.5 Hz. Ultrasound images, with 30 mm depth and at a frequency of 7 MHz with a dynamic range of 62 dB, were collected over three toe-raise cycles at a rate of approximately 60 frames per second, while marker coordinates were sampled at 100 Hz using eight Eagle cameras (Motion Analysis Corp.; Santa Rosa, CA). The above task was repeated three times, after which participants were asked to perform unloaded cyclical plantar- and dorsi-flexion motions at the same frequency while standing on the left leg with the right foot raised from the floor and extended in front; this motion was also repeated three times. These tasks were chosen to produce ranges of motion that were similar between the loaded and unloaded tasks and also similar to that of walking, without many of the attendant motions of the rest of the body that would occur during walking itself.

The ultrasound beamformer (Telemed LogicScan 128; Lithuania) produced a 5 V square-wave analog signal during image sampling. This signal was recorded using a data acquisition board (National Instruments PCIe-6259; Austin, TX) and Cortex software (Motion Analysis Corp.; Santa Rosa, CA) on the motion analysis system computer. The rising edge of this signal (plus an experimentally-determined time-delay) was used in subsequent analysis to synchronize the ultrasound images to the motion capture data.

ATma calculation: Ultrasound images of the Achilles tendon and marker locations were analyzed using a custom-written MATLAB (Mathworks Inc., Natick, MA) script. The superficial and deep tendon borders were located in each grayscale ultrasound image by first applying the histeq() histogram equalization transformation in MATLAB with two bins to obtain a black-and-white image. Borders parallel to the image margins between white and black regions were then found automatically by marching in the deep and superficial directions from an initial user-identified starting point in the center of the tendon. The tendon force line of action was taken to be the tendon midline that was midway between these two borders. The transmalleolar axis (TA) was defined as the line passing through the medial and lateral malleoli markers,

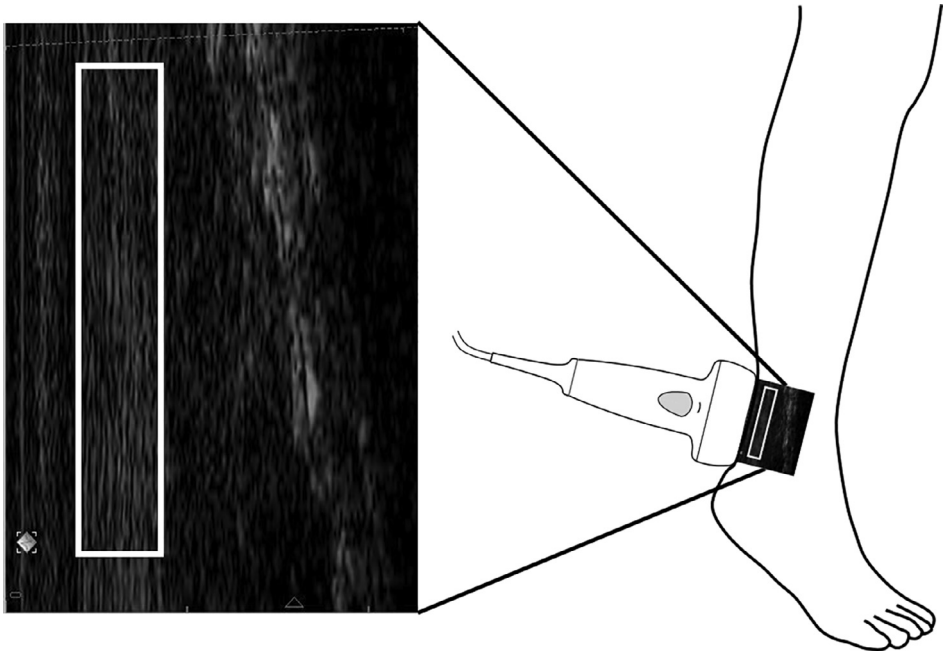

Fig. 1. Schematic illustration of ultrasound probe placement over the Achilles tendon, with a sample ultrasound image showing the Achilles tendon within the white box.

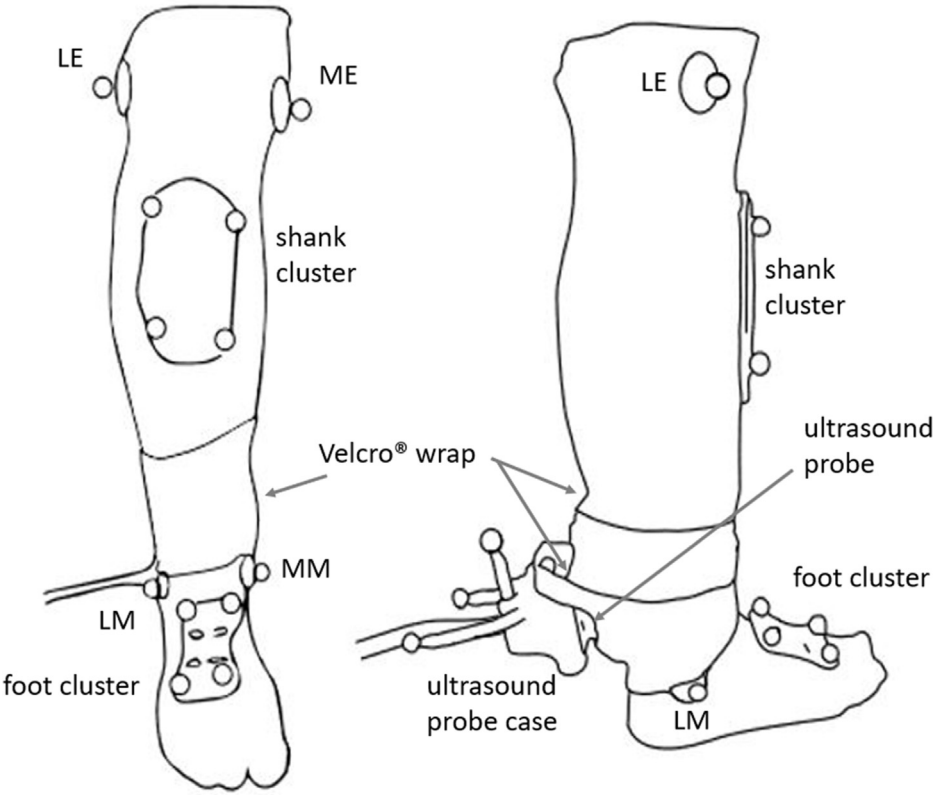

Fig. 2. Illustrations of the reflective markers attached to the skin of a subject along with the ultrasound probe affixed over the Achilles tendon using a custom probe-holder. Clusters of reflective markers were secured to the dorsum of the foot and the anterior shank, and individual markers were placed over the lateral and medial malleoli (LM and MM) and lateral and medial femoral epicondyles (LE and ME). An anterior view is shown on the left and a posterolateral view on the right.

while the coordinates of the transmalleolar midpoint (TM) were found as the spatial mean of the two malleoli.

The foot and shank coordinate systems were established following ISB recommendations (Wu et al., 2002). All marker coordinates were filtered using a bidirectional 4th order low-pass Butterworth filter with a cut-off frequency of 10 Hz. The coordinates of the foot and shank cluster markers were used to compute homogeneous transformations between the foot and shank segment coordinate systems using a least-squares fitting technique (Challis, 1995).

Finite helical axes were computed, at each time frame, using the shank-to-foot transformations from 25 frames (0.25 s) before and 25 frames after that time frame (Spoor and Veldpaus, 1980). As axes computed from skin-mounted markers are sensitive to noise when the magnitude of rotation is small, any helical axis for which the absolute value of the rotation about the axis was less than 0.2 rad was discarded (Woltring et al., 1985). A single axis representing the confluence (i.e, the "mean") of all the remaining helical axes was found using a previously described procedure (Lewis et al., 2006) and this axis was termed the "functional" axis (FA).

For the methods that made use of an axis of rotation (FA and TA) rather than a point center of rotation, ATma was computed by first finding the moment of a unit force $\vec{f}$ along the tendon line of action about an arbitrary point P on the axis of rotation:

$$\vec{M}_P = \overrightarrow{PQ} \times \vec{f} \quad (1)$$

where $\overrightarrow{PQ}$ is the vector pointing from P to an arbitrary point Q on the tendon line of action. Taking P′ to be a second point on the axis of rotation and $\vec{u}$ to be a unit vector along PP′, the moment of the unit tendon force about the axis was computed as the projection of $\vec{M}_P$ onto $\vec{u}$:

$$M_{PP'} = \vec{u} \cdot \left(\overrightarrow{PQ} \times \vec{f}\right) \quad (2)$$

Finally, ATma was found by shifting the terms in this scalar triple product and taking the absolute value to account for uncertainty in the direction of $\vec{u}$ along the axis of rotation:

$$ATma = \left|\overrightarrow{PQ} \cdot \left(\vec{u} \times \vec{f}\right)\right| \quad (3)$$

For the TM method, the shortest distance from the transmalleolar midpoint to the line of action of the Achilles tendon was computed and taken to be the ATma. Ankle joint angles were computed using ZXY Cardan decomposition (with Z being medial-lateral; X anterior-posterior; and Y superior-inferior) of the rotation matrices between the shank and foot coordinate systems at each time frame. Second-order polynomials were fit to plots of ATma versus plantarflexion-dorsiflexion angle and interpolations of these polynomials were used to estimate moment arms at 5° increments from +10° (dorsiflexion) to −20° (plantarflexion).

Statistical Analysis: A three-way repeated-measures ANOVA determined differences in ATma between methods (TA, TM, FA), loading conditions (loaded and unloaded) and ankle angle (+10°, +5°, 0°, −5°, −10°, −15°, and −20°) in SPSS (v23, IBM, USA) with the level of statistical significance set at $\alpha = 0.05$. When ANOVA indicated significance, simple effects *post hoc* analyses were conducted using a Bonferroni correction for multiple comparisons. Pairwise Pearson's correlations were computed between ATma assessed in neutral ankle position in both loading conditions to identify associations between ATma computed using the three methods.

3. Results

Mean ATma found using FA were significantly larger (all $p < 0.001$) than those from TA (mean differences of 14.0 mm and 9.5 mm for loaded and unloaded conditions, respectively) and TM (mean differences of 11.0 mm and 6.3 mm), while TM moment arms were larger than TA for loaded (mean difference of 3.0 mm, $p = 0.011$) and unloaded (mean difference of 3.2 mm, $p = 0.006$), Fig. 3). These patterns of differences were found across all joint angles examined ($p = 0.024$). The difference was most evident at 20° plantarflexion, for which FA values were 29% larger than TA values, and 24% larger than TM values, on average (Fig. 3).

When ATma was determined using the FA, a dependence on loading condition was observed. ATma from FA at maximum plantarflexion (20°) were on average 7.8 mm larger when loaded than when unloaded ($p < 0.001$). This significant difference remained for most comparisons but the effect was attenuated at smaller plantar flexion angles (all $p < 0.07$). As the ankle moved into dorsiflexion, however, no significant differences between loaded and unloaded ATma were observed for the FA method (all $p > 0.05$).

Loaded TA moment arms were marginally but not significantly larger (difference of 0.3 mm) than unloaded ($p = 0.523$). Within-angle comparisons revealed that loaded TA moment arms were not significantly different at any angle (all $p > 0.278$). There was a significant difference between TM moment arms measured at the two loading conditions at only the most plantarflexed position; loaded TM moment arms were 1.27 mm larger than unloaded ($p = 0.046$), but at no other angles were the differences significant.

ATma from FA in the loaded condition were found to increase in magnitude from 10° dorsiflexion to 20° plantarflexion (Table 1). When unloaded, ATma increased from neutral position to 20° plantarflexion. While some small but significant differences across joint angles were found for the TA and TM methods, the relationship between ATma and joint angle was less pronounced for TA and TM than for FA.

Pairwise Pearson's correlations between FA, TA and TM in an unloaded neutral position revealed significant relationships in each case (Fig. 4). Using standards set forth by Cohen (1988), TA and TM were strongly correlated ($r^2 = 0.853$, $p < 0.001$) while strong correlations were also found between FA and TM ($r^2 = 0.689$, $p < 0.001$),

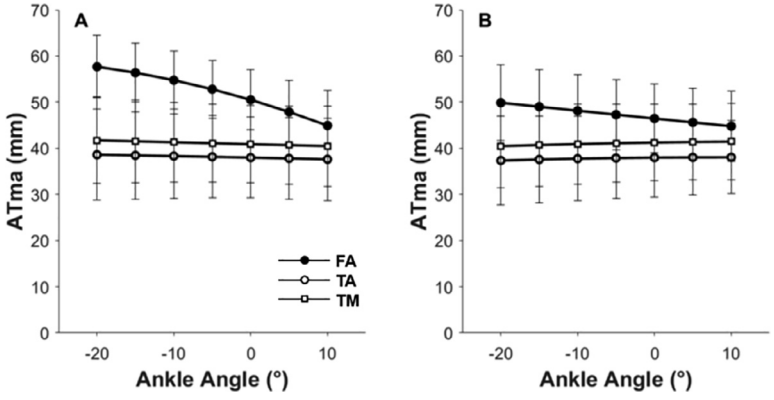

Fig. 3. Achilles tendon moment arms calculated with a 'functional' ankle rotation axis (FA, *filled circles*), a transmalleolar rotation axis (TA, *open circles*), or a transmalleolar midpoint (TM, *open squares*) in loaded (A) and unloaded (B) conditions, plotted versus ankle angle. Plantarflexion angles are negative and dorsiflexion angles are positive. Error bars indicate standard deviation (n = 15).

Table 1
Average differences between ATma values estimated at 20° plantarflexion, neutral, and 10° dorsiflexion for each loading condition found with each of the three methods (FA, TA, and TM). P-values are for Bonferroni-corrected post hoc mean comparisons between angles, with significant differences ($p < 0.05$) highlighted in bold type.

	FA loaded		FA unloaded		TA loaded		TA unloaded		TM loaded		TM unloaded	
Angle comparison	Mean difference (mm)	P-value	Mean difference (mm)	P-value	Mean difference (mm)	P-value	Mean difference (mm)	P-value	Mean difference (mm)	P-value	Mean difference (mm)	P-value
20° PF–10° DF	12.752	**<0.001**	5.099	**0.008**	0.983	1.000	−0.696	1.000	1.255	1.000	−0.989	1.000
20° PF–0°	7.177	**<0.001**	3.426	**0.001**	0.615	1.000	−0.628	1.000	0.842	1.000	−0.775	1.000
0–10° DF	5.575	**<0.001**	1.673	0.207	0.368	1.000	−0.068	1.000	0.413	1.000	−0.215	1.000

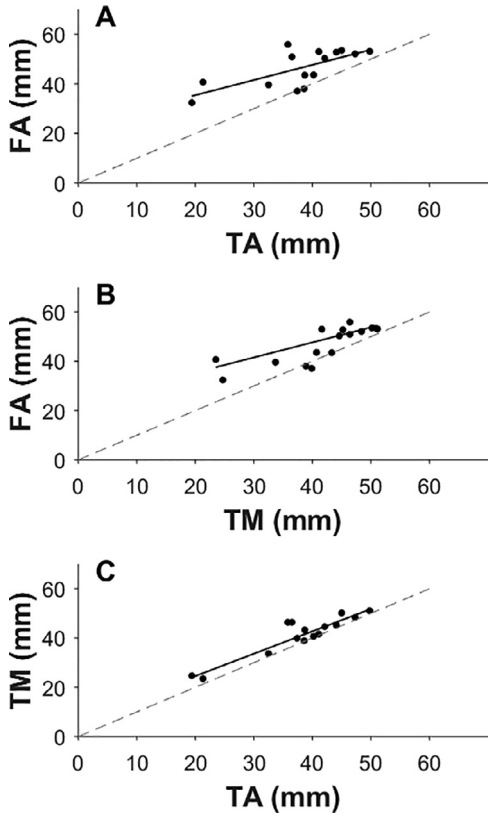

Fig. 4. Pairwise Pearson's correlations of Achilles tendon moment arm in neutral (0°) position and in the unloaded condition. Correlations were made between moment arms measured using different methods: (A) FA and TA ($r^2 = 0.474$, $p = 0.005$), (B) FA and TM ($r^2 = 0.689$, $p < 0.001$), and (C) TA and TM ($r^2 = 0.853$, $p < 0.001$). Lines of agreement ($y = x$) are displayed with gray dashes.

and FA and TA ($r^2 = 0.474$, $p = 0.005$). These correlations became slightly weaker for ATma measured in neutral position for the loaded condition (see supplementary Fig. S3 for these plots).

4. Discussion

Our estimates of ATma measured using an ultrasound-motion tracking hybrid method differed substantially when computed with an FA as compared those found using TA or TM representations of ankle joint axis or center of rotation (Fig. 3). Specifically, ATma from FA were larger, varied with plantarflexion angle more (such that ATma were larger in plantarflexion) and increased with loading to a greater extent. Estimates of ATma that approximated the ankle using anatomical landmarks (*i.e.*, TA or TM) did not vary appreciably with ankle joint angle or loading condition. Because the estimated position of the Achilles tendon was constant across the FA, TA, and TM methods, differences in ATma directly reflect differences in ankle axis position determined by those three methods.

To better understand why ATma computed with FA changed with joint angle and those computed with TA did not, we represented ATma as the product of two factors: (1) the shortest distance D (distance along the mutual perpendicular) between the tendon axis and each joint axis; and (2) a factor of sin β, where β is the angle between the tendon axis and the joint axis:

$$\mathrm{ATma} = D \sin \beta \tag{4}$$

Values of D and sin β for a representative subject are shown in Fig. 5. The shortest distance between the tendon and the FA varies considerably for both loaded and unloaded conditions, increasing with plantarflexion (Fig. 5A). However, the shortest distance between the tendon and TA varies considerably less, and shows a small increase with dorsiflexion. The angular differences between the tendon axis and either joint axis are small; the tendon is nearly perpendicular to both FA and TA (sin β nearly unity) throughout the range of motion (Fig. 5B). Variation in D over the range of motion for FA is due to the obliquity of the FA axis; this is evident in a three-dimensional plot of the FA, TA, and tendon axes in dorsiflexion and plantarflexion for this representative subject that we have included in the supplementary material (Fig. S4).

Our findings suggest that ATma estimated using FA provide a closer approximation of ATma estimated using MR-based geometric methods (Fig. 6). ATma that increased with plantarflexion were observed when using FA, a pattern similar to that previously reported in 2D MR studies (Fath et al., 2010; Hashizume et al., 2012; Maganaris et al., 1998; Rugg et al., 1990). The same pattern was not observed when using TA or TM, commensurate with previously published results using a similar method (Manal et al., 2013; Rasske et al., 2017). The results from previous studies presented in Fig. 6 along with the results of the present study suggest that ATma measured using techniques in which the center or axis of rotation is located based on ankle motion are larger than ATma measured using a center or axis of rotation defined by the malleoli. It is important to note, however, that comparisons of ATma magnitude across investigations must be interpreted with caution because ATma differences may be attributable in part to differences among participant groups such as body size.

Loading condition influenced ATma computed with FA (Fig. 3), in agreement with findings from MR studies. We found a 10% increase in FA moment arm for our loaded condition as compared to unloaded across all joint angles. Maganaris et al. (1998) reported a 22–27% increase in ATma from MR between rest and maximal voluntary contraction (MVC) of the triceps surae, which they attributed to a change in tendon orientation due to muscle bulging with contraction. Hashizume et al. (2014) reported an approximately 15% increase in ATma with 30% of maximum effort. The toe-raise activity we used for our loaded condition likely did not produce maximal contractions, suggesting that our findings are in line with these previous studies. As in previous studies using the TM method, we measured only a small change (0.2%) in ATma

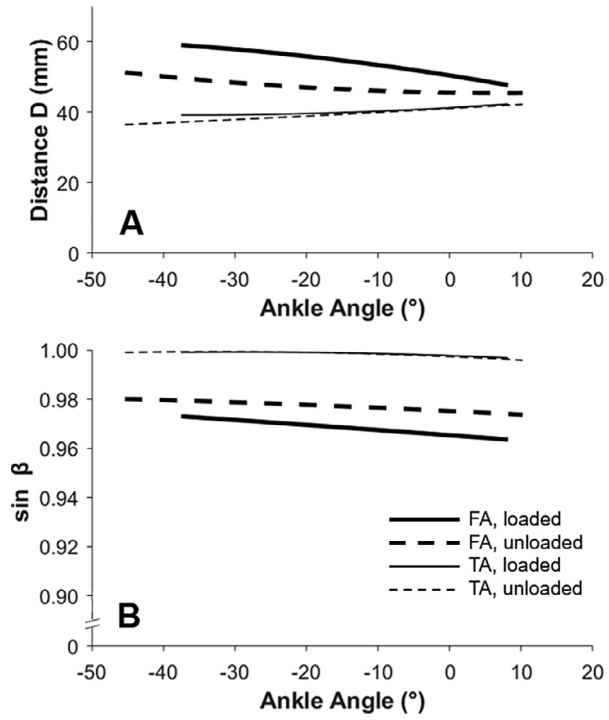

Fig. 5. (A) The shortest distance D between the functional axis (FA, *thick lines*) or transmalleolar axis (TA, *thin lines*) and the Achilles tendon for both loaded (solid) and unloaded (dashed) conditions for individual trials of a representative subject. (B) The sine of the angle (β) between these same axes. Variation in ATma with joint angle seen for FA but not TA was primarily attributable to variation in D with joint angle.

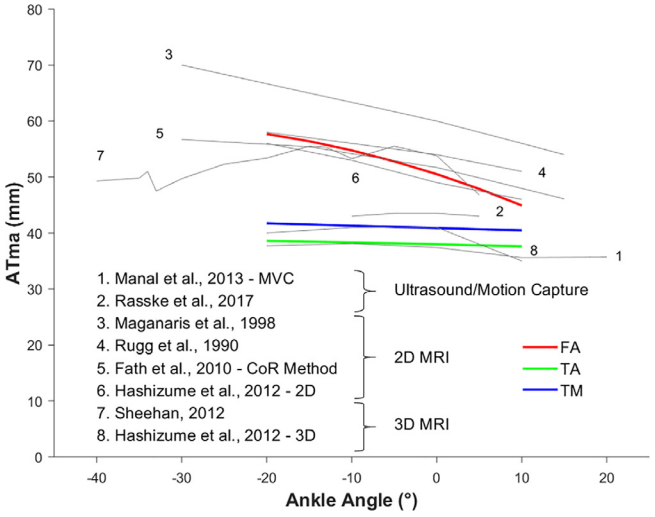

Fig. 6. Loaded Achilles tendon moment arms found using a functional axis (FA, *red*), transmalleolar axis (TA, *green*), and a transmalleolar midpoint (TM, *blue*), plotted versus ankle angle. As in Fig. 3, plantarflexion angles are negative and dorsiflexion angles are positive. Moment arm values from previous studies, computed using ultrasound/motion capture (1 and 2), 2D MRI (3– 6), and 3D MRI (7 and 8), are plotted in gray.

between loaded and unloaded conditions. Manal et al. (2013) noted a 3.5% difference between MVC and passive conditions when using the TM method.

The functional axis (FA) and the transmalleolar axis and midpoint (TA and TM) were in roughly the same location for each participant, so it was perhaps unsurprising that the ATma estimated in neutral ankle position derived using these three methods were strongly correlated with one another (Fig. 4). Only a little more than half the variance in FA moment arm was explained by TM or TA, however, suggesting that ATma found using FA were not simply scaled-up versions of their TM and TA counterparts. The bone kinematic measurements of Lundberg et al. (1989) showed TM to be a good approximation of the intersection of the tibiotalar axes of rotation derived throughout the range of ankle motion. It may be that variation in rotation axis orientation not captured when TM is used affects ATma estimates in important ways. Similarly, the findings of Lundberg et al. (1989) show that the ankle plantarflexion axis of rotation is similar to TA in the transverse plane, but when projected onto the sagittal plane, substantial differences in axis inclination with TA were observed. The findings of Lundberg et al. (1989) are in agreement with other studies of bone kinematics (Isman and Inman, 1969; Lundberg, 1989; Sammarco et al., 1973).

Certain limitations affected this study, including the assumption that the Achilles tendon force line of action is located midway between the superficial and deep tendon borders. We computed FA from clusters of markers mounted on the tibia and the dorsum of the foot. As such, it is likely that the tibia-to-foot transformations included motions other than ankle motions, including talocalcaneal motion, tarsal and tarsometatarsal joint motion, and skin movement relative to the bones. The confounding effects of some of these extraneous motions could have been avoided if we had placed our foot cluster on the heel, but we found it difficult to do so without interfering with the ultrasound probe cluster. Foot deformation with foot loading may be substantial (Leardini et al., 2007; Xiong et al., 2009), and it is possible that the observed differences in ATma between loading conditions for FA are an artefact of such foot deformation rather than differences in rotation axes. It is possible that inconsistency in the placement of the probe relative to the tendon could have contributed to variability in our moment arm estimates. When we tested the same subjects on different days, however, the differences in moment arm were typically 1–2 mm, a level of repeatability that we deemed acceptable relative to the differences in moment arm noted between the two methods and across our subjects.

The FA we used was a single fixed axis but studies of bone kinematics show that the axis of tibiotalar rotation moves throughout the range of ankle motion (Lundberg, 1989; Lundberg et al., 1989). We chose a fixed axis in the present study so that we could make a more direct comparison to the fixed transmalleolar axis (TA). Future work will build on the present study by considering the effects of using a moving instantaneous helical axis on estimates of ATma, as has been done in previous 3D MR studies (Sheehan, 2012, 2010).

Representing ankle joint axis of rotation with a functional axis derived from relative motions of the foot and shank produced ATma that increased in magnitude with plantarflexion and loading, and was larger than those obtained from anatomical landmarks. ATma estimated using anatomical landmark representations of the ankle (TA and TM) failed to show substantial variation with either joint angle or loading condition.

Conflict of interest

The authors have no conflicts of interest to declare.

Funding

Funding for this research was provided by the Herbert A. and Jean V. Barron International Scholars Fund at Penn State University.

Appendix A. Supplementary material

Supplementary data to this article can be found online at https://doi.org/10.1016/j.jbiomech.2019.04.032.

References

Baxter, J.R., Piazza, S.J., 2014. Plantar flexor moment arm and muscle volume predict torque-generating capacity in young men. J. Appl. Physiol. 116, 538–544. https://doi.org/10.1152/japplphysiol.01140.2013.

Carrier, D.R., Heglund, N.C., Earls, K.D., 1994. Variable gearing during locomotion in the human musculoskeletal system. Science 265, 651–653. https://doi.org/10.1126/science.8036513.

Challis, J.H., 1995. A procedure for determining rigid body transformation parameters. J. Biomech. 28, 733–737. https://doi.org/10.1016/0021-9290(94)00116-L.

Clarke, E.C., Martin, J.H., d'Entremont, A.G., Pandy, M.G., Wilson, D.R., Herbert, R.D., 2015. A non-invasive, 3D, dynamic MRI method for measuring muscle moment arms in vivo: demonstration in the human ankle joint and Achilles tendon. Med. Eng. Phys. 37, 93–99. https://doi.org/10.1016/j.medengphy.2014.11.003.

Cohen, J., 1988. The significance of a product moment rs. In: Cohen, J. (Ed.), Statistical Power Analysis for the Behavioral Sciences. 2nd ed. Academic Press, pp. 75–107. https://doi.org/10.1016/B978-0-12-179060-8.50008-6.

Fath, F., Blazevich, A.J., Waugh, C.M., Miller, S.C., Korff, T., 2010. Direct comparison of in vivo Achilles tendon moment arms obtained from ultrasound and MR scans. J. Appl. Physiol. 109, 1644–1652. https://doi.org/10.1152/japplphysiol.00656.2010.

Franz, J.R., Khanchandani, A., McKenny, H., Clark, W.H., 2018. Ankle rotation and muscle loading effects on the calcaneal tendon moment arm: an in vivo imaging and modeling study. Biomed. Eng. Ann. https://doi.org/10.1007/s10439-018-02162-4.

Hashizume, S., Iwanuma, S., Akagi, R., Kanehisa, H., Kawakami, Y., Yanai, T., 2014. The contraction-induced increase in Achilles tendon moment arm: a three-dimensional study. J. Biomech. 47, 3226–3231. https://doi.org/10.1016/j.jbiomech.2014.08.003.

Hashizume, S., Iwanuma, S., Akagi, R., Kanehisa, H., Kawakami, Y., Yanai, T., 2012. In vivo determination of the Achilles tendon moment arm in three-dimensions. J. Biomech. 45, 409–413. https://doi.org/10.1016/j.jbiomech.2011.10.018.

Isman, R.E., Inman, V.T., 1969. Anthropometric studies of the human foot and ankle. Foot Ankle 11, 97–129.

Ito, M., Akima, H., Fukunaga, T., 2000. In vivo moment arm determination using B-mode ultrasonography. J. Biomech. 33, 215–218.

Leardini, A., Benedetti, M.G., Berti, L., Bettinelli, D., Nativo, R., Giannini, S., 2007. Rear-foot, mid-foot and fore-foot motion during the stance phase of gait 25, 453–462, doi: 10.1016/j.gaitpost.2006.05.017.

Lewis, G.S., Sommer, H.J., Piazza, S.J., 2006. In vitro assessment of a motion-based optimization method for locating the talocrural and subtalar joint axes. J. Biomech. Eng. 128, 596. https://doi.org/10.1115/1.2205866.

Lieber, R.L., Ward, S.R., 2011. Skeletal muscle design to meet functional demands. Philos. Trans. R. Soc. B Biol. Sci. 366, 1466–1476. https://doi.org/10.1098/rstb.2010.0316.

Lundberg, A., 1989. Kinematics of the ankle and foot. In vivo roentgen stereophotogrammetry. Acta Orthop. Scand. Suppl. 233, 1–24. https://doi.org/10.3109/17453678909154185.

Lundberg, A., Svensson, O.K., 1993. The axes of rotation of the talocalcaneal and talonavicular joints. Foot 3, 65–70. https://doi.org/10.1016/0958-2592(93)90064-A.

Lundberg, A., Svensson, O.K., Nemeth, G., Selvik, G., 1989. The axis of rotation of the ankle joint. J. Bone Jt. Surgery, Br. vol. 71–B, 94–99.

Maganaris, C.N., 2004. Imaging-based estimates of moment arm length in intact human muscle-tendons. Eur. J. Appl. Physiol. 91, 130–139. https://doi.org/10.1007/s00421-003-1033-x.

Maganaris, C.N., Baltzopoulos, V., Sargeant, A.J., 2000. In vivo measurement-based estimations of the human Achilles tendon moment arm. Eur. J. Appl. Physiol. 83, 363–369. https://doi.org/10.1007/s004210000247.

Maganaris, C.N., Baltzopoulos, V., Sargeant, A.J., 1998. Changes in Achilles tendon moment arm from rest to maximum isometric plantarflexion: in vivo observations in man. J. Physiol. 510, 977–985. https://doi.org/10.1016/S0268-0033(99)00018-2.

Manal, K., Cowder, J.D., Buchanan, T.S., 2013. Subject-specific measures of Achilles tendon moment arm using ultrasound and video-based motion capture. Physiol. Rep. 1,. https://doi.org/10.1002/phy2.139 e00139.

Manal, K., Cowder, J.D., Buchanan, T.S., 2010. A hybrid method for computing achilles tendon moment arm using ultrasound and motion analysis. J. Appl. Biomech. 26, 224–228. https://doi.org/10.1016/j.bbi.2008.05.010.

Olszewski, K., Dick, T.J.M., Wakeling, J.M., 2015. Achilles tendon moment arms: the importance of measuring at constant tendon load when using the tendon excursion method. J. Biomech. 48, 1206–1209. https://doi.org/10.1016/j.jbiomech.2015.02.007.

Rasske, K., Thelen, D.G., Franz, J.R., 2017. Variation in the human Achilles tendon moment arm during walking. Comput. Methods Biomech. Biomed. Engin. 20, 201–205. https://doi.org/10.1080/10255842.2016.1213818.

Rugg, S.G., Gregor, R.J., Mandelbaum, B.R., Chiu, L., 1990. In vivo moment arm calculations at the ankle using magnetic resonance imaging (MRI). J. Biomech. 23, 495–501. https://doi.org/10.1016/0021-9290(90)90305-M.

Sammarco, G., Burstein, A., Frankel, V., 1973. Biomechanics of the ankle: a kinematic study. Proc. Am. Orthop. Foot Soc. Inc. 4, 75–96.

Sammarco, J., 1977. Biomechanics of the ankle. I. Surface velocity and instant centre of rotation in the sagittal place. Am. J. Sports Med. 5, 231–234. https://doi.org/10.1177/036354657700500603.

Sheehan, F.T., 2012. The 3D in vivo Achilles' tendon moment arm, quantified during active muscle control and compared across sexes. J. Biomech. 45, 225–230. https://doi.org/10.1016/j.jbiomech.2011.11.001.

Sheehan, F.T., 2010. The instantaneous helical axis of the subtalar and talocrural joints: a non-invasive in vivo dynamic study. J. Foot Ankle Res. 3, 13. https://doi.org/10.1186/1757-1146-3-13.

Siston, R.A., Daub, A.C., Giori, N.J., Goodman, S.B., Delp, S.L., 2005. Evaluation of methods that locate the center of the ankle for computer-assisted total knee arthroplasty. Clin. Orthop. Relat. Res. 129–135. https://doi.org/10.1097/01.blo.0000170873.88306.56.

Spoor, C.W., van Leeuwen, J.L., 1992. Knee muscle moment arms from MRI and from tendon travel. J. Biomech. 25, 201–206. https://doi.org/10.1016/0021-9290(92)90276-7.

Spoor, C.W., Veldpaus, F.E., 1980. Rigid body motion calculated from spatial co-ordinates of markers. J. Biomech. 13, 391–393. https://doi.org/10.1016/0021-9290(80)90020-2.

Storace, A., Wolf, B., 1979. Functional analysis of the role of the finger tendons. J. Biomech. 12, 575–578.

Takahashi, K.Z., Gross, M.T., Van Werkhoven, H., Piazza, S.J., Sawicki, G.S., 2016. Adding stiffness to the foot modulates soleus force-velocity behaviour during human walking. Sci. Rep. 6, 1–11. https://doi.org/10.1038/srep29870.

Woltring, H.J., Huiskes, R., de Lange, A., Veldpaus, F.E., 1985. Finite centroid and helical axis estimation from noisy landmark measurements in the study of human joint kinematics. J. Biomech. 18, 379–389. https://doi.org/10.1016/0021-9290(85)90293-3.

Wu, G., Siegler, S., Allard, P., Kirtley, C., Leardini, A., Rosenbaum, D., Whittle, M., D'Lima, D.D., Cristofolini, L., Witte, H., Schmid, O., Stokes, I., 2002. ISB recommendation on definitions of joint coordinate system of various joints for the reporting of human joint motion—part I: ankle, hip, and spine. J. Biomech. 35, 543–548. https://doi.org/10.1016/S0021-9290(01)00222-6.

Xiong, S., Oonetilleke, R.S.G., Hao, J.Z., Wenyan, L.I., Itana, C.P.W., 2009. Foot deformations under different load-bearing conditions and their relationships to stature and body weight. Anthropol. Sci. 117, 77–88. https://doi.org/10.1537/ase.070915.